nessa publishers

Journal of Geology & Earth Sciences
Volume 1| Issue 6

Review Article **Open Access**

On similarity of Seismo Magnetic Moment and pressure Head Fractal Dimension for Characterizing Shajara Reservoirs of the Permo-Carboniferous Shajara Formation, Saudi Arabia

Khalid Elyas Mohamed Elameen Alkhidir

*__Corresponding author__: Khalid Elyas Mohamed Elameen Alkhidir, Department of Petroleum and Natural Gas Engineering, College of Engineering, King Saud University, Saudi Arabia; Email: kalkhidir@ksu.edu.sa

Citation: Khalid Elyas Mohamed Elameen Alkhidir (2020) On similarity of Seismo Magnetic and pressure Head Fractal Dimension for Characterizing Shajara Reservoirs of the Permo-Carboniferous Shajara Formation, Saudi Arabia : Nessa Journal Geology & Earth Sciences.

Abstract

The quality and assessment of a reservoir can be documented in details by the application of seismo magnetic moment. This research aims to calculate fractal dimension from the relationship among seismo magnetic moment, maximum seismo magnetic moment and wetting phase saturation and to approve it by the fractal dimension derived from the relationship among inverse pressure head * pressure head and wetting phase saturation. Two equations for calculating the fractal dimensions have been employed. The first one describes the functional relationship between wetting phase saturation, seismo magnetic moment, maximum seismo magnetic moment and fractal dimension. The second equation implies to the wetting phase saturation as a function of pressure head and the fractal dimension. Two procedures for obtaining the fractal dimension have been utilized. The first procedure was done by plotting the logarithm of the ratio between seismo magnetic moment and maximum seismo magnetic moment versus logarithm wetting phase saturation. The slope of the first procedure = 3- Df (fractal dimension). The second procedure for obtaining the fractal dimension was determined by plotting the logarithm (inverse of pressure head and pressure head) versus the logarithm of wetting phase saturation. The slope of the second procedure = Df -3. On the basis of the obtained results of the fabricated stratigraphic column and the attained values of the fractal dimension, the sandstones of the Shajara reservoirs of the Shajara Formation were divided here into three units.

Keywords: Shajara Reservoirs, Shajara Formation, Seismo magnetic moment fractal dimension, Capillary pressure fractal dimension

Introduction

Seismo electric effects related to electro kinetic potential, dielectric permittivity, pressure gradient, fluid viscosity, and electric conductivity was first reported by [1]. Capillary pressure follows the scaling law at low wetting phase saturation was reported by [2]. Seismo electric phenomenon by considering electro kinetic coupling coefficient as a function of effective charge density, permeability, fluid viscosity and electric conductivity was reported by [3]. The magnitude of seismo electric current depends on porosity, pore size, zeta potential of the pore surfaces, and elastic properties of the matrix was investigated by [4]. The tangent of the ratio of converted electric field to pressure is approximately in inverse proportion to permeability was studied by [5]. Permeability inversion from seismoelectric log at low frequency was studied by [6]. They reported that, the tangent of the ratio among electric excitation intensity and pressure field is a function of porosity, fluid viscosity, frequency, tortuosity and fluid density and Dracy permeability. A decrease of seismo electric frequencies with increasing water content was reported by [7]. An increase of seismo electric transfer function with increasing water saturation was studied by [8]. An increase of dynamic seismo electric transfer function with decreasing fluid conductivity was described by [9]. The amplitude of seismo electric signal increases with increasing permeability which means that the seismo electric effects are directly related to the permeability and can be used to study the permeability of the reservoir was illustrated by [10]. Seismo electric coupling is frequency dependent and decreases exponentially when frequency increases was demonstrated by [11]. An increase of permeability with increasing seismo magnetic moment and seismo diffusion coefficient fractal dimension was reported by [12, 13]. An increase of, molar enthalpy, work, electro kinetic, bubble pressure and pressure head fractal dimensions with permeability increasing and grain size was described by [14, 15, 16, 17].

Material and method

Sandstone samples were collected from the surface type section of the Permo-Carboniferous Shajara Formation, latitude 26° 52' 17.4", longitude 43° 36' 18". (Figure1). Porosity was measured on collected samples using mercury intrusion Porosimetry and permeability was derived from capillary pressure data. The purpose of this paper is to obtain Seismo magnetic moment fractal dimension and to confirm it by pressure head fractal dimension. The fractal dimension of the first procedure is determined from the positive slope of the plot of logarithm of the ratio of Seismo magnetic moment to maximum Seismo magnetic moment log ($SMM^{1/4}/SMM^{1/4}_{max}$) versus log wetting phase saturation (logSw). Whereas the fractal dimension of the second procedure is determined from the negative slope of the plot of logarithm of log (inverse of pressure head α * pressure head h, log (α * h) versus logarithm of wetting phase saturation (log Sw).

The Seismo magnetic moment can be scaled as

$$\mathbf{Sw} = \left[\frac{\mathbf{SMM}^{\frac{1}{4}}}{\mathbf{SMM}_{\mathbf{max}}^{\frac{1}{4}}}\right]^{[\mathbf{3-Df}]} \qquad (\mathbf{1})$$

Where Sw the water saturation, SMM the seismo magnetic moment in ampere * square meter, SMM_{max} the maximum seismo magnetic moment in ampere * square meter, and Df the fractal dimension.

Equation 1 can be proofed from

$$\mathbf{H} = \left[\frac{\boldsymbol{\phi} * \boldsymbol{\epsilon} * \mathbf{kf} * \boldsymbol{\zeta} * \boldsymbol{\rho}\mathbf{f} * \mathbf{SSWV} * \mathbf{SRGV}}{\boldsymbol{\alpha}\infty * \boldsymbol{\eta}}\right] \qquad (\mathbf{2})$$

Where H the Seismo magnetic field in ampere / meter, ϕ the porosity, ϵ the fluid permittivity in Faraday / meter, kf the fluid dielectric constant, the fluid density Pf in kilogram / cubic meter, SSWV the seismic shear wave velocity in meter / second, SRGV the seismo radial grain velocity in meter / second, α∞ the tortuosity, η the fluid viscosity in pascal * second

The Seismo magnetic field H can be scaled as

$$\mathbf{H} = \left[\frac{\mathbf{i}}{\mathbf{d}}\right] \qquad (\mathbf{3})$$

Where H the Seismo magnetic field in ampere /meter, i the electric current in ampere, d the distance in meter

Insert equation 3 into equation 2

$$\left[\frac{\mathbf{i}}{\mathbf{d}}\right] = \left[\frac{\boldsymbol{\phi} * \boldsymbol{\epsilon} * \mathbf{kf} * \boldsymbol{\zeta} * \boldsymbol{\rho}\mathbf{f} * \mathbf{SSWV} * \mathbf{SRGV}}{\boldsymbol{\alpha}\infty * \boldsymbol{\eta}}\right] \qquad (\mathbf{4})$$

The electric current can be scaled as

$$\mathbf{i} = \left[\frac{\mathbf{SMM}}{\mathbf{A}}\right] \qquad (\mathbf{5})$$

Where i the electric current in ampere, SSM the seismo magnetic moment in ampere * square meter, A the area in meter

Insert equation 5 into equation 4

$$\left[\frac{\mathbf{SMM}}{\mathbf{d} * \mathbf{A}}\right] = \left[\frac{\boldsymbol{\phi} * \boldsymbol{\epsilon} * \mathbf{kf} * \boldsymbol{\zeta} * \boldsymbol{\rho}\mathbf{f} * \mathbf{SSWV} * \mathbf{SRGV}}{\boldsymbol{\alpha}\infty * \boldsymbol{\eta}}\right] \qquad (\mathbf{6})$$

The area can be scaled as

$$\mathbf{A} = \left[\frac{\mathbf{Q} * \boldsymbol{\eta} * \mathbf{L}}{\mathbf{k} * \boldsymbol{\Delta}\mathbf{p}}\right] \qquad (\mathbf{7})$$

Where A the area in square meter, Q the flow rate in cubic meter / second, η the fluid viscosity in pascal * second, L the capillary length in meter, k the permeability in square meter, Δp the differential pressure in pascal.

Insert equation 7 into equation 6

$$\left[\frac{\mathbf{SMM} * \mathbf{k} * \boldsymbol{\Delta}\mathbf{p}}{\mathbf{d} * \mathbf{Q} * \boldsymbol{\eta} * \mathbf{L}}\right] = \left[\frac{\boldsymbol{\phi} * \boldsymbol{\epsilon} * \mathbf{kf} * \boldsymbol{\zeta} * \boldsymbol{\rho}\mathbf{f} * \mathbf{SSWV} * \mathbf{SRGV}}{\boldsymbol{\alpha}\infty * \boldsymbol{\eta}}\right] \qquad (\mathbf{8})$$

Equation 8 after rearrange will become

$$\left[\frac{\mathbf{SMM} * \mathbf{k} * \mathbf{\Delta p}}{\mathbf{d} * \boldsymbol{\eta} * \mathbf{L}}\right] = \left[\frac{\boldsymbol{\phi} * \boldsymbol{\epsilon} * \mathbf{kf} * \boldsymbol{\zeta} * \boldsymbol{\rho}\mathbf{f} * \mathbf{SSWV} * \mathbf{SRGV} * \mathbf{Q}}{\boldsymbol{\alpha}\infty * \boldsymbol{\eta}}\right] \quad (9)$$

The flow rate can be scaled as

$$\mathbf{Q} = \left[\frac{\mathbf{3.14} * \mathbf{r^4} * \mathbf{\Delta p}}{\mathbf{8} * \boldsymbol{\eta} * \mathbf{L}}\right] \quad (10)$$

Where Q the flow rate in cubic meter / second, r the pore radius in meter, Δp the differential pressure in pascal, η the fluid viscosity in pascal * second, and L the capillary length in meter.

Insert equation 10into equation 9

$$\left[\frac{\mathbf{SMM} * \mathbf{k} * \mathbf{\Delta p}}{\mathbf{d} * \boldsymbol{\eta} * \mathbf{L}}\right] = \left[\frac{\boldsymbol{\phi} * \boldsymbol{\epsilon} * \mathbf{kf} * \boldsymbol{\zeta} * \boldsymbol{\rho}\mathbf{f} * \mathbf{SSWV} * \mathbf{SRGV} * \mathbf{3.14} * \mathbf{r^4} * \mathbf{\Delta p}}{\boldsymbol{\alpha}\infty * \boldsymbol{\eta} * \mathbf{8} * \boldsymbol{\eta} * \mathbf{L}}\right] \quad (11)$$

The maximum pore radius can be scaled a

$$\left[\frac{\mathbf{SMM_{max}} * \mathbf{k} * \mathbf{\Delta p}}{\mathbf{d} * \boldsymbol{\eta} * \mathbf{L}}\right] = \left[\frac{\boldsymbol{\phi} * \boldsymbol{\epsilon} * \mathbf{kf} * \boldsymbol{\zeta} * \boldsymbol{\rho}\mathbf{f} * \mathbf{SSWV} * \mathbf{SRGV} * \mathbf{3.14} * \mathbf{r\_max4} * \mathbf{\Delta p}}{\boldsymbol{\alpha}\infty * \boldsymbol{\eta} * \mathbf{8} * \boldsymbol{\eta} * \mathbf{L}}\right] \quad (12)$$

Divide equation 11 by equation 12

$$\left[\frac{\left[\frac{\mathbf{SMM} * \mathbf{k} * \mathbf{\Delta p}}{\mathbf{d} * \boldsymbol{\eta} * \mathbf{L}}\right]}{\left[\frac{\mathbf{SMM_{max}} * \mathbf{k} * \mathbf{\Delta p}}{\mathbf{d} * \boldsymbol{\eta} * \mathbf{L}}\right]}\right] = \left[\frac{\left[\frac{\boldsymbol{\phi} * \boldsymbol{\epsilon} * \mathbf{kf} * \boldsymbol{\zeta} * \boldsymbol{\rho}\mathbf{f} * \mathbf{SSWV} * \mathbf{SRGV} * \mathbf{3.14} * \mathbf{r^4} * \mathbf{\Delta p}}{\boldsymbol{\alpha}\infty * \boldsymbol{\eta} * \mathbf{8} * \boldsymbol{\eta} * \mathbf{L}}\right]}{\left[\frac{\boldsymbol{\phi} * \boldsymbol{\epsilon} * \mathbf{kf} * \boldsymbol{\zeta} * \boldsymbol{\rho}\mathbf{f} * \mathbf{SSWV} * \mathbf{SRGV} * \mathbf{3.14} * \mathbf{r\_max4} * \mathbf{\Delta p}}{\boldsymbol{\alpha}\infty * \boldsymbol{\eta} * \mathbf{8} * \boldsymbol{\eta} * \mathbf{L}}\right]}\right] \quad (13)$$

Equation 13 after simplification will become

$$\left[\frac{\mathbf{SSM}}{\mathbf{SMM_{max}}}\right] = \left[\frac{\mathbf{r^4}}{\mathbf{r_{max}^4}}\right] \quad (14)$$

Take the fourth root of equation 14

$$\sqrt[4]{\left[\frac{\mathbf{r^4}}{\mathbf{r_{max}^4}}\right]} = \sqrt[4]{\left[\frac{\mathbf{SSM}}{\mathbf{SMM_{max}}}\right]} \quad (15)$$

Equation 15 after simplification will become

$$\left[\frac{\mathbf{r}}{\mathbf{r_{max}}}\right] = \left[\frac{\mathbf{SSM^{\frac{1}{4}}}}{\mathbf{SSM_{max}^{\frac{1}{4}}}}\right] \quad (16)$$

Take the logarithm of equation 16

$$\log\left[\frac{r}{r_{max}}\right] = \log\left[\frac{SSM^{\frac{1}{4}}}{SSM_{max}^{\frac{1}{4}}}\right] \quad (17)$$

$$\text{But; } \log\left[\frac{r}{r_{max}}\right] = \left[\frac{\log Sw}{3 - Df}\right] \quad (18)$$

Insert equation 18 into equation 17

$$\left[\frac{\log Sw}{3 - Df}\right] = \log\left[\frac{SSM^{\frac{1}{4}}}{SSM_{max}^{\frac{1}{4}}}\right] \quad (19$$

Equation 19 after log removal will become

$$Sw = \left[\frac{SSM^{\frac{1}{4}}}{SSM_{max}^{\frac{1}{4}}}\right]^{[3-Df]} \quad (20)$$

Equation 20 the proof of equation 1 which relates the water saturation, seismo magnetic moment, maximum seismo magnetic moment, and the fractal dimension.

The pressure head can be scaled as

$$LogSw = [Df - 3] * \log(\alpha * h) + constant \quad (21)$$

Where Sw the water saturation, α inverse of pressure head, h the pressure head and Df the fractal dimension.

Results and Discussion

Based on field observation the Shajara Reservoirs of the Permo-Carboniferous Shajara Formation were divided here into three units as described in Figure1.These units from bottom to top are: Lower Shajara Reservoir, Middle Shajara reservoir, and Upper Shajara Reservoir. Their attained results of the seismo magnetic moment fractal dimension and pressure head fractal dimension are shown in Table 1. Based on the achieved results it was found that the seismo magnetic moment fractal dimension is equal to the pressure head fractal dimension. The maximum value of the fractal dimension was found to be 2.7872 allocated to sample SJ13 from the Upper Shajara Reservoir as verified in Table 1. Whereas the minimum value of the fractal dimension 2.4379 was reported from sample SJ3 from the Lower Shajara reservoir as shown in Table1. The Seismo magnetic moment fractal dimension and pressure head fractal dimension were detected to increase with increasing permeability as proofed in Table1 owing to the possibility of having interconnected channels.

The Lower Shajara reservoir was symbolized by six sandstone samples (Figure 1), four of which label as SJ1, SJ2, SJ3 and SJ4 were carefully chosen for capillary pressure measurement as proven in Table1. Their positive slopes of the first procedure log of the Seismo magnetic moment to maximum Seismo magnetic moment versus log wetting phase saturation (Sw) and negative slopes of the second procedure log (inverse of pressure head α*pressure head h)

versus log wetting phase saturation (Sw) are clarified in Figure 2, Figure 3, Figure 4, Figure 5 and Table 1. Their Seismo magnetic moment fractal dimension and pressure head fractal dimension values are revealed in Table 1. As we proceed from sample SJ2 to SJ3 a pronounced reduction in permeability due to compaction was described from 1955 md to 56 md which reflects decrease in Seismo magnetic moment fractal dimension from 2.7748 to 2.4379 as quantified in table 1. Again, an increase in grain size and permeability was proved from sample SJ4 whose Seismo magnetic moment fractal dimension and pressure head fractal dimension was found to be 2.6843 as described in Table 1.

In contrast, the Middle Shajara reservoir which is separated from the Lower Shajara reservoir by an unconformity surface as revealed in Figure 1. It was nominated by four samples (Figure 1), three of which named as SJ7, SJ8, and SJ9 as illuminated in Table1 were chosen for capillary measurements as described in Table 1. Their positive slopes of the first procedure and negative slopes of the second procedure are shown in Figure 6, Figure 7 and Figure 8 and Table 1. Furthermore, their Seismo magnetic moment fractal dimensions and pressure head fractal dimensions show similarities as defined in Table 1.Their fractal dimensions are higher than those of samples SJ3 and SJ4 from the Lower Shajara Reservoir due to an increase in their permeability as explained in table 1.

On the other hand, the Upper Shajara reservoir was separated from the Middle Shajara reservoir by yellow green mudstone as shown in Figure 1. It is defined by three samples so called SJ11, SJ12, and SJ13 as explained in Table 1. Their positive slopes of the first procedure and negative slopes of the second procedure are displayed in Figure 9, Figure 10 and Figure 11 and Table 1. Moreover, their Seismo magnetic moment fractal dimension and pressure head fractal dimension are also higher than those of sample SJ3 and SJ4 from the Lower Shajara Reservoir due to an increase in their permeability as simplified in table 1.

Overall a plot of positive slope of the first procedure versus negative slope of the second procedure as described in Figure 12 reveals three permeable zones of varying Petro physical properties. These reservoir zones were also confirmed by plotting Seismo magnetic moment fractal dimension versus pressure head fractal dimension as described in Figure 13. Such variation in fractal dimension can account for heterogeneity which is a key parameter in reservoir quality assessment.

Conclusion

The sandstones of the Shajara Reservoirs of the permo-Carboniferous Shajara Formation were divided here into three units based on seismo magnetic moment fractal dimension. The Units from base to top are: Lower Shajara Seismo Magnetic Moment Fractal Dimension Unit, Middle Shajara Seismo Magnetic Moment Fractal Dimension Unit, and Upper Shajara Seismo Magnetic Moment Fractal Dimension Unit. These units were also proved by pressure head fractal dimension. The fractal dimension was found to increase with increasing grain size and permeability owing to possibility of having interconnected channels.

Acknowledgement

The author would to thank King Saud University, college of Engineering, Department of Petroleum and Natural Gas Engineering, Department of Chemical Engineering, Research Centre at College of Engineering, College of science, Department of Geology and Geophysics, and King Abdullah Institute for research and Consulting Studies for their supports.

References

1. Frenkel J. 1944, on the theory of seismic and seismoelectric phenomena in a moist soil. Journal of physics 3, 230-241.

2. Li K, Williams W.2007, Determination of pressure head function from resistivity data. Transport in Porous Media 67, 1-15.

3. Revil A, Jardani A. 2010, Seismo electric response of heavy oil reservoirs: theory and numerical modeling. Geophysical Journal International 180, 781-797.

4. Dukhin A, Goetz P, Thommes M. 2010, Seismoelectric effect: a non-isochoric streaming current.1 Experiment. Journal of Colloid and Interface Science 345, 547-553.

5. Guan W, Hu H, Wang Z. 2012, Permeability inversion from low-frequency seismoelectric logs in fluid-saturated porous formations. Geophysical Prospecting 61, 120-133.

6. Hu H, Guan W, Zhao W. 2012, Theoretical studies of permeability inversion from seismoelectric logs. Geophysical Research Abstracts 14, EGU2012-6725-1 2012 EGU General Assembly.

7. Borde C, S en echal P Barri`ere J, Brito D, Normandin E et al.,2015, Impact of water saturation on seismoelectric transfer functions: a laboratory study of co-seismic phenomenon. Geophysical J International 200, 1317-1335.

8. Jardani A, Revil A (2015) Seismoelectric couplings in a poroelastic material containing two immiscible fluid phases. Geophysical Journal International 202, 850-870.

9. Holzhauer J, Brito D, Bordes C, Brun Y, Guatarbes B. 2016, Experimental quantification of the seismoelectric transfer function and its dependence on conductivity and saturation in loose sand. Geophysical Prospecting 65, 1097-1120

10. RongPeng, Jian-Xing Wei, Bang-Rang Di, Pin-Bo Ding, ZiChun Liu (2016) Experimental research on seismoelectric effects in sandstone. Applied Geophysics 13, 425-436.

11. Djuraev U, Jufar S R, Vasant P. 2017, Numerical Study of frequency-dependent seismo electric coupling in partially saturated porous media. MATEC Web of Conferences 87, 02001.

12. Alkhidir KEME. 2020, Seismo Magnetic Moment Fractal Dimension for Characterizing Shajara Reservoirs of the Permo Carboniferous Shajara Formation, Saudi Arabia World Scientific News 139 (2),186-200.

13. Alkhidir KEME. 2019, Seismo Diffusion Coefficient Fractal Dimension for Characterizing Shajara Reservoirs of the Permo-Carboniferous Shajara Formation, Saudi Arabia. Research Journal of Nano science and Engineering 3 (4), 23-29.

14. Alkhidir KEME. 2019, Molar Enthalpy Fractal Dimension for Characterizing Shajara Reservoirs of the Permo-Carboniferous Shajara Formation. Journal of Agriculture and Aquaculture 1(1),1-8.

15. Alkhidir KEME. 2019, Work Fractal Dimension for Characterizing Shajara Reservoirs of the Permo Carboniferous Shajara Formation, Saudi Arabia. International Journal of Environment & Agricultural Science 3(2),1-8

16. Alkhidir KEME.2018, Electro Kinetic Fractal Dimension for Characterizing Shajara Reservoirs of the Shajara Formation. International Journal of Nanotechnology in Medicine & Engineering 3(4),54-60

17. Al-Khidir KE.2018, On Similarity of Pressure Head and Bubble Pressure Fractal Dimensions for Characterizing Permo-Carboniferous Shajara Formation, Saudi Arabia. Journal of Industrial Pollution and Toxicity 1(1), 102

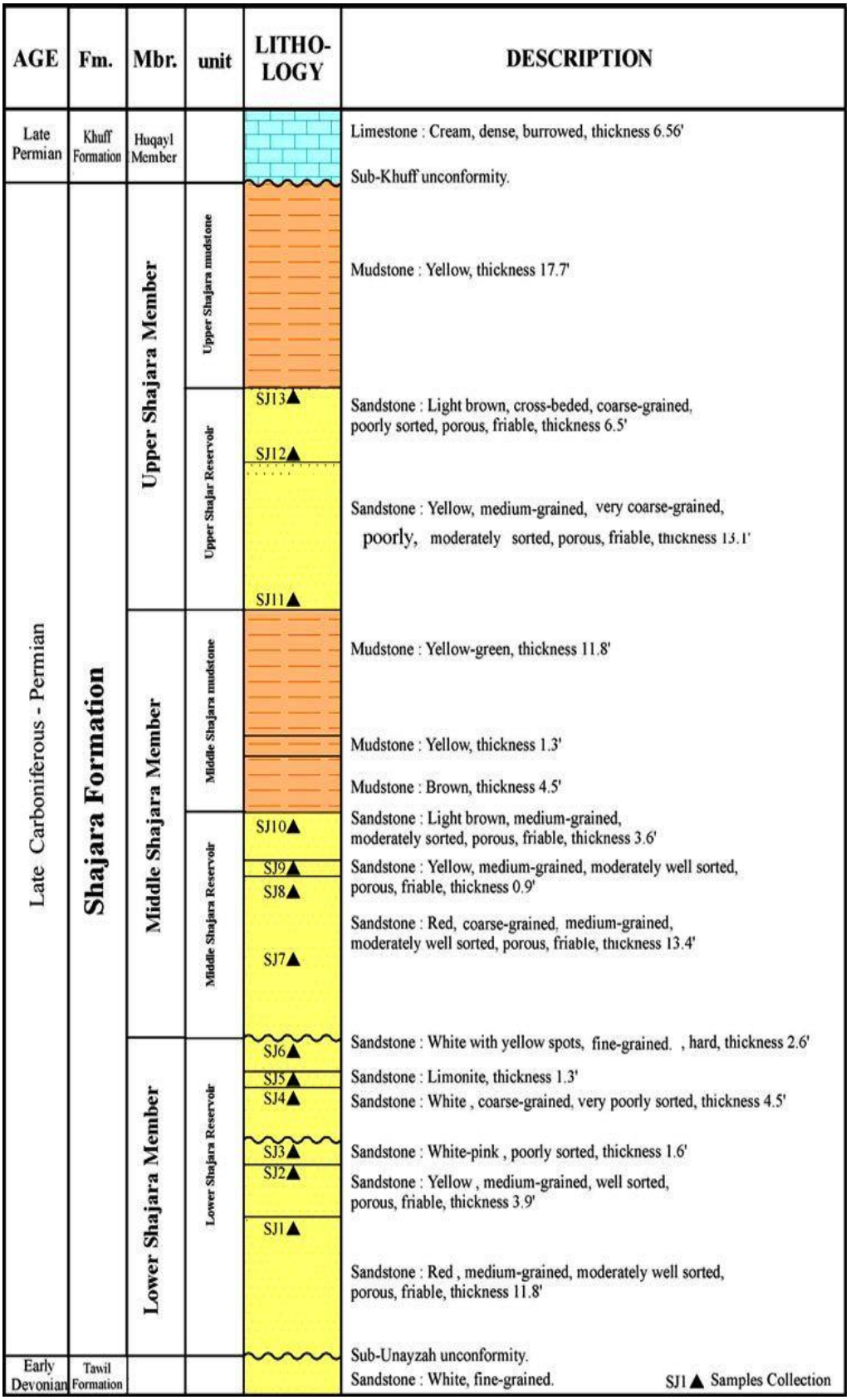

Figure 1: Surface type section of the Shajara Reservoirs of the Permo-Carboniferous Shajara Formation at latitude 26° 52' 17.4" longitude 43° 36' 18"

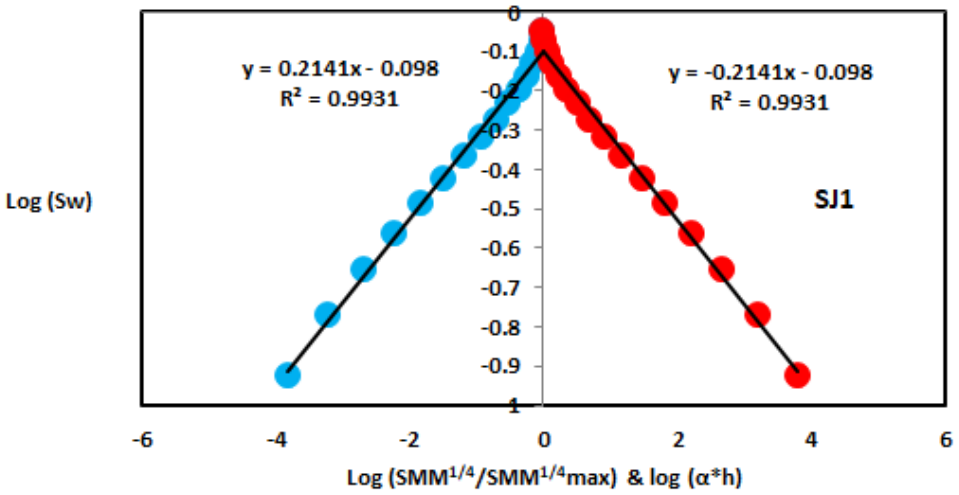

Figure 2: Log ($SMM^{1/4}/SMM^{1/4}_{max}$) & log (α*h) versus log Sw for sample SJ1

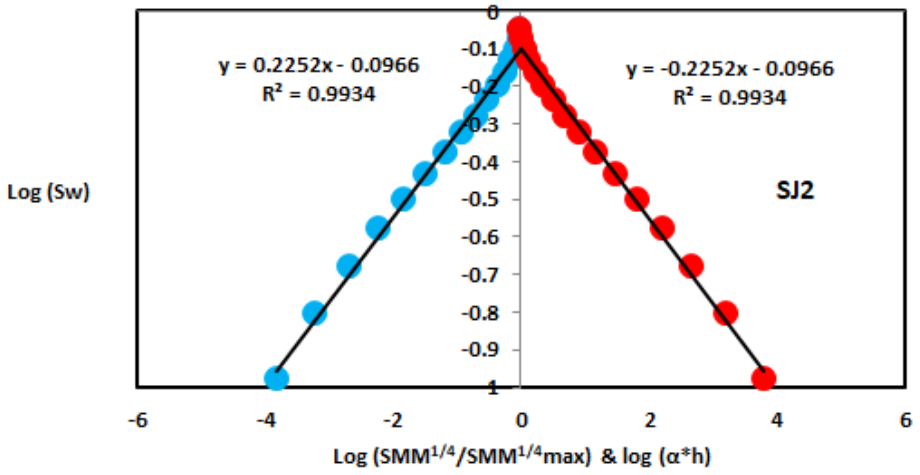

Figure 3: Log ($SMM^{1/4}/SMM^{1/4}_{max}$) & log (α*h) versus log Sw for sample SJ2

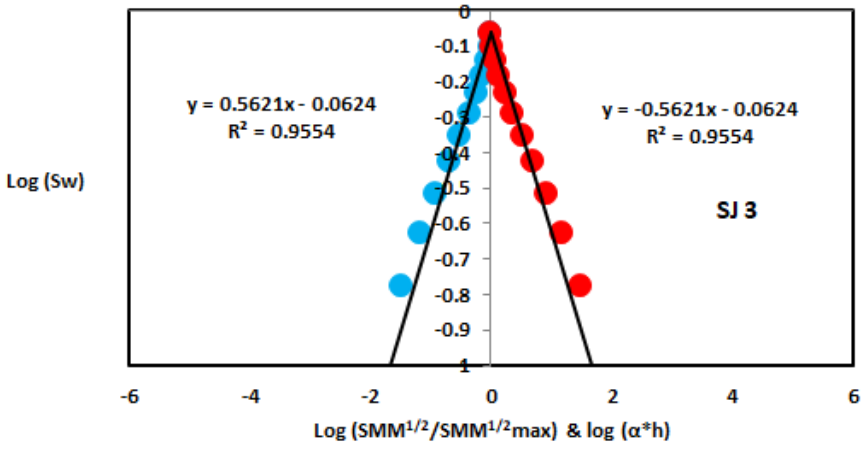

Figure 4: Log ($SMM^{1/4}/SMM^{1/4}_{max}$) & log (α*h) versus log Sw for sample SJ3

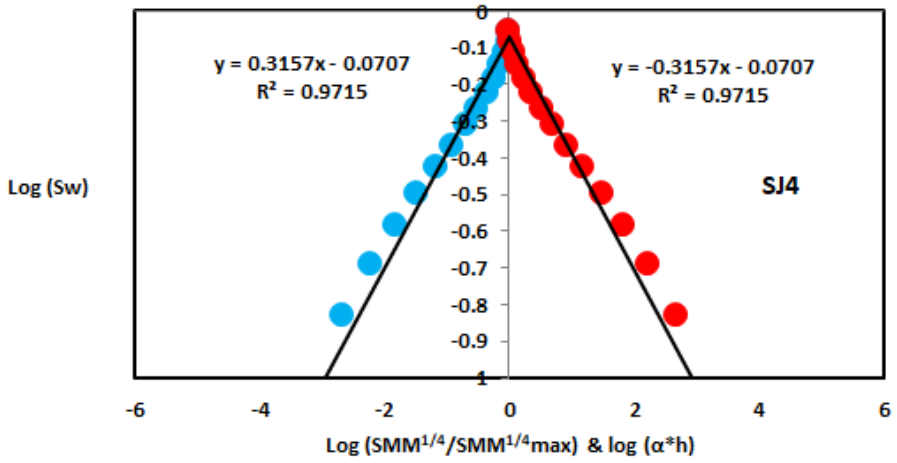

Figure 5: Log ($SMM^{1/4}/SMM^{1/4}_{max}$) & log (α*h) versus log Sw for sample SJ4

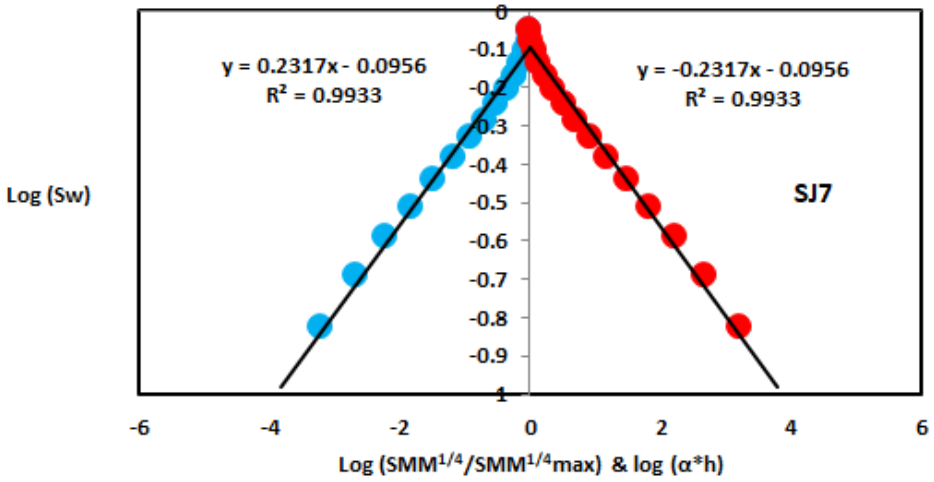

Figure 6: Log ($SMM^{1/4}/SMM^{1/4}_{max}$) & log (α*h) versus log Sw for sample SJ7

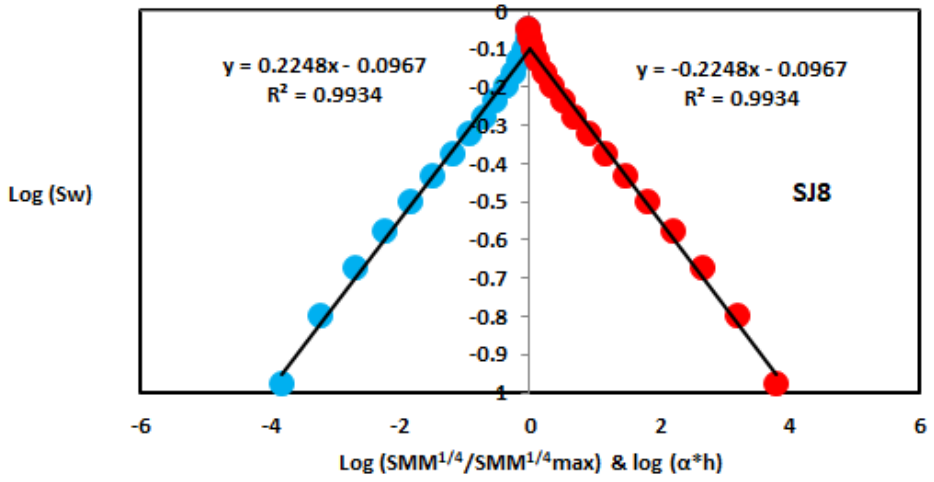

Figure 7: Log ($SMM^{1/4}/SMM^{1/4}_{max}$) & log (α*h) versus log Sw for sample SJ8

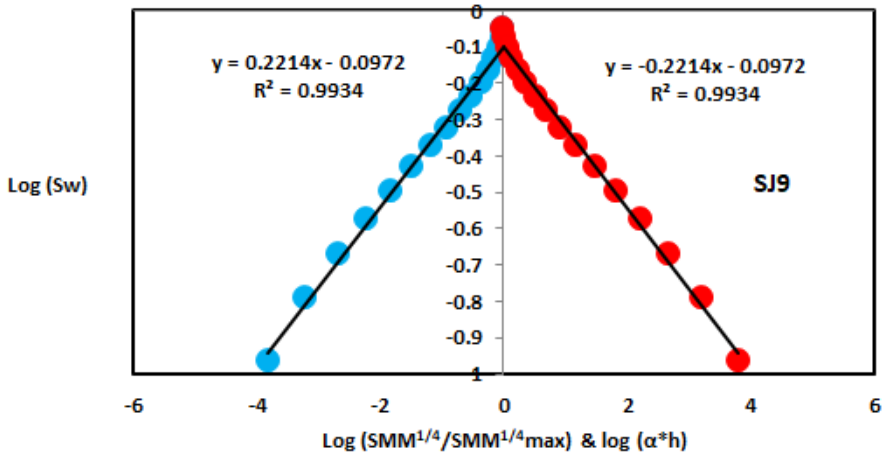

Figure 8: Log ($SMM^{1/4}/SMM^{1/4}_{max}$) & log (α*h) versus log Sw for sample SJ9

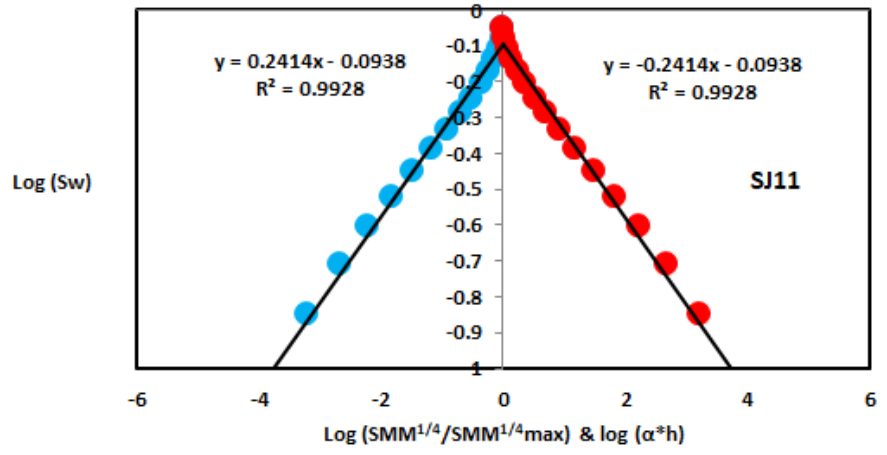

Figure 9: Log ($SMM^{1/4}/SMM^{1/4}_{max}$) & log (α*h) versus log Sw for sample SJ11

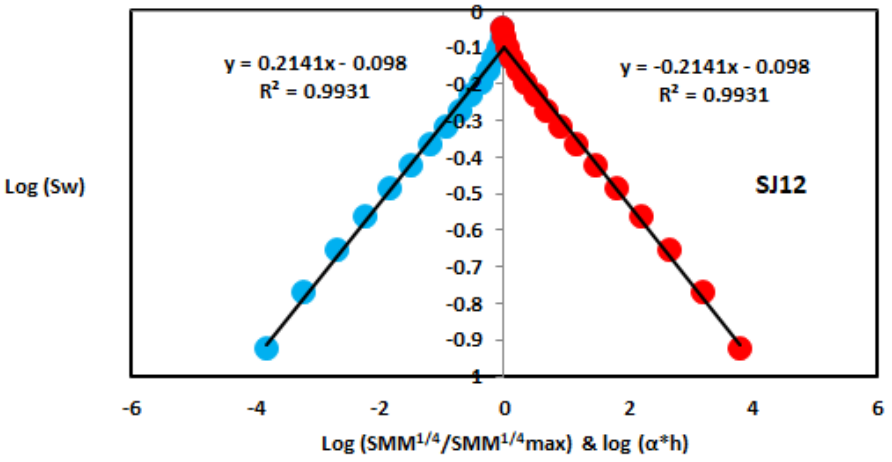

Figure10: Log ($SMM^{1/4}/SMM^{1/4}_{max}$) & log (α*h) versus log Sw for sample SJ12

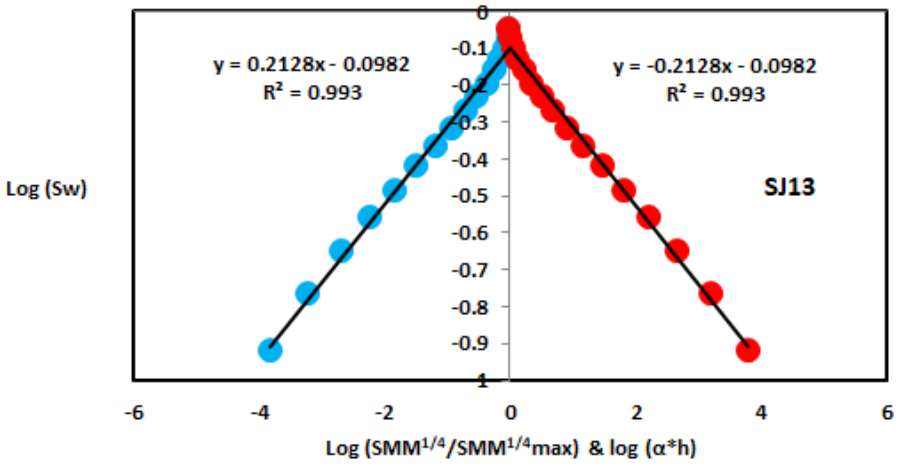

Figure11: Log ($SMM^{1/4}/SMM^{1/4}_{max}$) & log (α*h) versus log Sw for sample SJ13

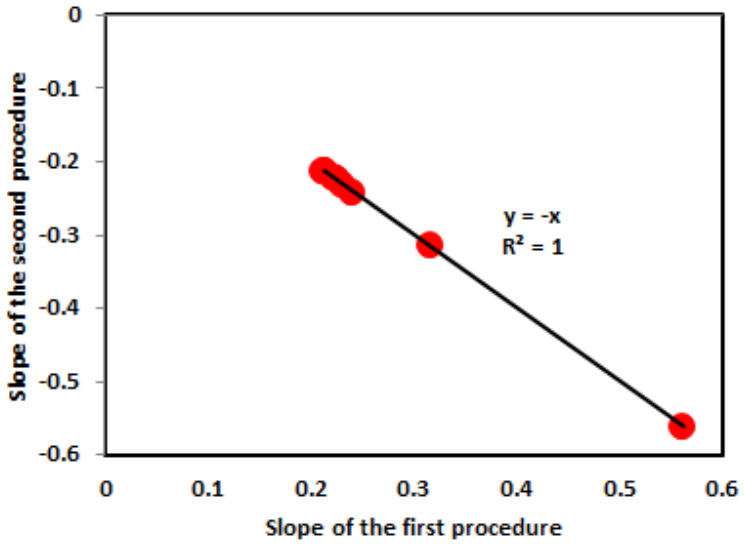

Figure12: Slope of the first procedure versus slope of the second procedure

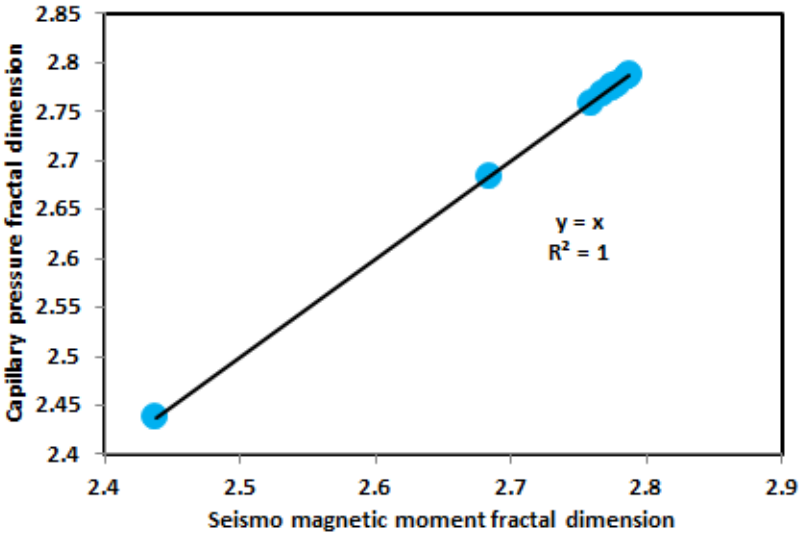

Figure13: Seismo magnetic moment fractal dimension versus pressure head fractal dimension

Table 1: Petrophysical model showing the three Shajara Reservoir Units with their corresponding values of seismo magnetic moment fractal dimension and pressure head fractal dimension

Formation	Reservoir	Sample	Porosity %	k (md)	Positive slope of the first procedure Slope=3-Df	Negative slope of the second procedure Slope=Df-3	Seismo magnetic moment fractal dimension	Pressure head fractal dimension
Permo-Carboniferous Shajara Formation	Upper Shajara Reservoir	SJ13	25	973	0.2128	-0.2128	2.7872	2.7872
		SJ12	28	1440	0.2141	-0.2141	2.7859	2.7859
		SJ11	36	1197	0.2414	-0.2414	2.7586	2.7586
	Middle Shajara Reservoir	SJ9	31	1394	0.2214	-0.2214	2.7786	2.7786
		SJ8	32	1344	0.2248	-0.2248	2.7752	2.7752
		SJ7	35	1472	0.2317	-0.2317	2.7683	2.7683
	Lower Shajara Reservoir	SJ4	30	176	0.3157	-0.3157	2.6843	2.6843
		SJ3	34	56	0.5621	-0.5621	2.4379	2.4379
		SJ2	35	1955	0.2252	-0.2252	2.7748	2.7748
		SJ1	29	1680	0.2141	-0.2141	2.7859	2.7859